Effect of longitudinal stiffeners' spacing in lateral-torsional buckling

Néstor I. Prado (Main and Corresponding Author)
Civil Engineering Faculty, Universidad Pontificia Bolivariana
Km 7 via Piedecuesta, Bucaramanga (Colombia)
nestor.prado@upb.edu.co
https://orcid.org/0000-0002-8259-8995

Julian Carrillo
Civil Engineering Department, Universidad Militar Nueva Granada
Km 2 via Cajicá-Zipaquirá, Bogotá (Colombia)
julian.carrillo@unimilitar.edu.co
https://orcid.org/0000-0002-8274-5414

Sergio M. Pineda
Civil Engineering Faculty,Universidad Pontificia Bolivariana
Km 7 via Piedecuesta, Bucaramanga (Colombia)
sergio.pineda@upb.edu.co
https://orcid.org/0000-0001-6333-9878

Manuscript Code: 13448
Date of Acceptance/Reception: 23.11.2020/08.05.2020
DOI: 10.7764/RDLC.19.3.190

Abstract
This study focused on the experimental assessment of the effect of the spacing between longitudinal stiffeners welded to I-shaped beams under the action of lateral-torsional buckling. In this procedure, 192 aluminum beams on a 1:9 scale were tested under simple-support conditions with a laterally unbraced length ranging from 0.55 m through 1.95 m. Moreover, the stiffeners' spacing was also ranged from 3 to 9 times the depth of section. The structural behavior of the beams is discussed in terms of their flexural capacity, spacing between longitudinal stiffeners, lateral displacement of compression flange and failure angle twist. Results show that the spacing of longitudinal stiffeners influences the flexural capacity of I-shaped beams, so that, when the spacing of longitudinal stiffeners decreases, flexural capacity tends to increase, especially in the elastic buckling zone.

Keywords: longitudinal stiffeners, lateral-torsional buckling, I-shaped beam, flexural capacity, failure twist angle.

Introduction

The structural behavior on I-shaped beams with longitudinal stiffeners has been studied in several investigations in order to enhance flexural capacity. The use of the I-shaped beams with longitudinal stiffeners solely near the supports was evaluated by Hotchkiss (1966) and Vacharajittiphan & Trahair (1974, 1975) as shown in Figure 1(a).

On the other hand Plum Carsten & Svensson Sven Eilif (1993) analytically evaluated the behavior of I-shaped beams with box-type stiffeners as shown Figure 1(b), welded to web and flanges of section. The resistance of longitudinal, box-type, transversal and cross stiffeners as shown in Figures 1(a)-(d) respectively, were studied numerically by Szewczak Richard et al. (1983). These authors reported that the transversal stiffeners exhibited the lowest efficiency, whereas the box-type stiffeners showed the highest efficiency. The four aforementioned types of stiffeners were also assessed by Murtha-Smith Erling (1995), who studied the effect of using cross stiffeners on one, both, and alternating sides of the web, as well.

Figure 1. Stiffeners types. **a)** Longitudinal stiffeners; **b)** Box stiffeners; **c)** Transversal stiffeners; **d)** Cross stiffeners; **e)** Diagonal stiffeners. (adapted from Smith, 1995).

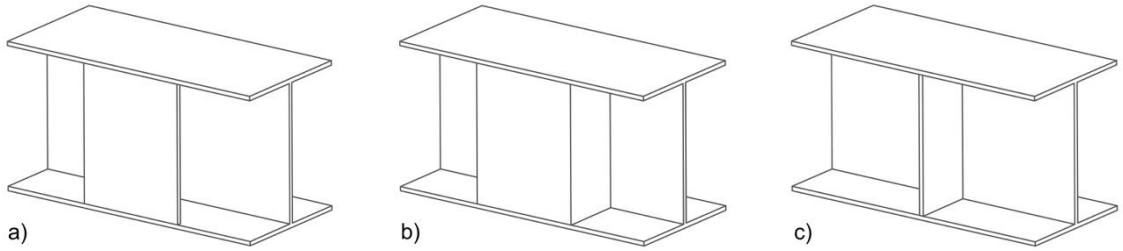

The use of channels as stiffeners, resembling a box-type stiffener as shown in Figure 1(b), was also studied by Ojalvo (1975, 1980) and Heins & Potocko (1979). Last researchers presented two analytical methods, one with approximations and another with rigorous supposition. Ojalvo & Chambers (1977) evaluated the effect of box-type stiffeners located only at the ends of the beam. In addition, these authors' work evaluated diagonal stiffeners as shown in Figure 1(e). Takabatake (1988) and Takabatake Hideo et al. (1991) theoretically and experimentally demonstrated the flexure capacity of the I-shaped beams with longitudinal and transverse stiffeners arranged arbitrarily.

Recently Cakiroglu et al. (2020) optimized the cross-sections of plate girders using the called harmony search algorithm. This meta-heuristic model rigorous achieved to reduce the cross-sectional area up to 16% with respect to original specimen, which generates savings in material and construction costs. Mamazizi et al. (2013) numerical and experimentally evaluated the behavior of the post-buckling of steel plate girders subjected to shear considering both rigid and non-rigid transversal stiffeners. The results of this work were compared against the Eurocode3 specifications.

Finally, Prado et al. (2018) experimentally evaluated the use of longitudinal stiffeners with different laterally unbraced lengths L_b. The tests in this study were performed using only a spacing of 420 mm between longitudinal stiffeners, which represented an *e/d* ratio of 3, defined as the center-to-center spacing of the stiffeners divided by the depth of the section. The study reports an increment in the flexural capacity for each laterally unbraced length L_b, and left the open idea that it would be interesting to know the increase in flexural capacity for different spacing of longitudinal stiffeners.

Therefore, this work focused on the experimental evaluation of the improvement of flexural capacity in I-shaped beams achieved by using different spacings between longitudinal stiffeners and laterally unbraced lengths L_b. Due to the quantity of test specimens required in this study, the I-shaped aluminum beams were selected with a 1:9 scaling to carry out the tests. The expected improvement is evaluated in terms of the measured flexural capacity and the lateral-torsional buckling experienced by the specimens, both beneficial for the design of laterally-unbraced large beams.

Experimental program

The experimental program of this study was accomplished at the Laboratory of Structures at Universidad Pontificia Bolivariana in Bucaramanga, Colombia, where a hundred ninety two (192) I-shaped aluminum beams were flexural strength testing, whose dimensions and geometrical properties are shown in Figure 2 and Table 1, respectively.

Figure 2. Dimensions of test specimens. (Self-Elaboration).

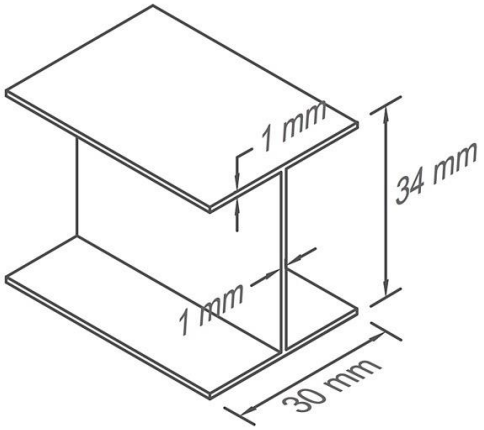

Table 1. Geometrical properties of the cross-section. (Self-Elaboration).

	Strong axis				Weak axis					
A (mm^2)	Ix (mm^4)	Sx (mm^3)	rx (mm)	Zx (mm^3)	Iy (mm^4)	Sy (mm^3)	ry (mm)	Zy (mm^3)	J (mm^4)	Cw (mm^6)
92	19071	1122	14	1246	4503	300	7	458	31	1225851

Geometrical properties were calculated according to equations of the mechanical of materials (Gere & Goodno, 2013; Salmon et al., 2009).

The moment of inertia, I_x and I_y, were calculated according to Eqs. 1 and 2,

$$I_x = 2\left[\left(\frac{b_f t_f^3}{12}\right) + b_f t_f \left(\frac{d}{2} - \frac{t_f}{2}\right)^2\right] + \frac{t_w h_w^3}{12} \quad (1)$$

$$I_y = 2\left(\frac{t_f b_f^3}{12}\right) + \frac{h_w t_w^3}{12} \quad (2)$$

Where,
d = Overall depth of section
b_f = Flange width
t_w = Web thickness
t_f = Flange thickness
h_w = Depth of web

The elastic section modulus, S_x and S_y, were calculated according to Eqs. 3 and 4,

$$S_x = \frac{I_x}{d/2} \quad (3)$$

$$S_y = \frac{I_y}{b_f/2} \quad (4)$$

The radius of gyration, r_x and r_y, were calculated according to Eqs. 5 and 6,

$$r_x = \sqrt{I_x/A} \quad (5)$$

$$r_y = \sqrt{I_y/A} \quad (6)$$

The plastic modulus, Z_x and Z_y, were calculated according to Eqs. 7 and 8,

$$Z_x = 2\left[b_f\, t_f \left(\frac{d}{2} - \frac{t_f}{2}\right)\right] + 2\left(t_w \frac{h_w}{2} \frac{h_w}{4}\right) \quad (7)$$

$$Z_y = 4\left(t_f \frac{b_f}{2} \frac{b_f}{4}\right) + 2\left(h_w \frac{t_w}{2} \frac{t_w}{4}\right) \quad (8)$$

The torsion constant, J, was calculated according to Eq. 9,

$$J = \frac{1}{3}\left(2\, b_f\, t_f^3 + h_w t_w^3\right) \quad (9)$$

The torsional warping constant, C_w, was calculated according to Eq. 10,

$$C_w = \frac{I_y\, h_o^2}{4} \quad (10)$$

Where,
h_o = Distance between the flange centroids

The I-shaped beams satisfied the permissible tolerances in cross-section and longitudinal straightness (camber and Sweep) in accordance with ASTM A6/A6M (American Society for Testing and Materials, A01 Committee, 2016).

Table 2. Mechanical properties of the beams. (Self-Elaboration).

Yield strength (MPa)	Ultimate strength (MPa)	Ultimate strain (%)	Modulus of elasticity (MPa)
106.6	122.4	8.6	78699.8

The mechanical properties average of the aluminum beams (Table 2) were measured through four tension test in material samples taken from the specimens as it is shown in Figure 3, and they were performed according with the requirements of ASTM B557 (American Society for Testing and Materials, B07 Committee, 2015).

Figure 3. Sample extraction for stress test. (Self-Elaboration).

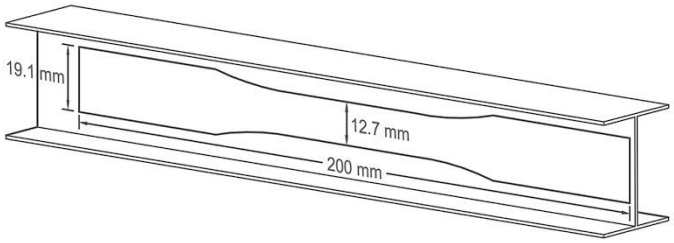

In concordance with the limit of width-to-thickness ratio of flange λ_p and web λ_r, the sections are classified as compact web and non-compact flanges. The limits of width-to-thickness ratio were calculated using the requirements of ANSI/AISC 360 (American Institute of Steel Construction, 2016) and listed in Table 3.

Table 3. Width-to-thickness ratio in the beams. (Self-Elaboration).

Flange			Web		
Width-to-thickness ratio	Limiting width-to-thickness ratio For compact λ_p	For noncompact λ_r	Width-to-thickness ratio	Limiting width-to-thickness ratio For compact λ_p	For Noncompact λ_r
$\frac{b_f}{2t_f}$	$0.38\sqrt{E/f_y}$	$1.0\sqrt{E/f_y}$	$\frac{h}{t_w}$	$3.76\sqrt{E/f_y}$	$5.70\sqrt{E/f_y}$
15	10.3	27.2	32	102.2	154.9
Non-compact flange section			Compact web section		

The laterally unbraced length L_b that separates plastic buckling from inelastic buckling (L_p = 0.55 m), and inelastic buckling from elastic buckling (L_r = 1.0 m), were calculated according with the requirements of ANSI/AISC 360 (2016). The bending tests were performed using separation between supports of 0.55, 0.80, 1.00, 1.20, 1.40, 1.60, 1.80 and 1.95 m.

Figure 4. Longitudinal stiffeners location schema. (Self-Elaboration).

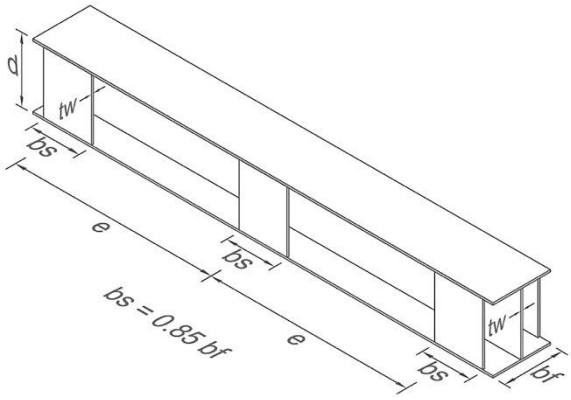

Longitudinal stiffeners were welded to the top and bottom edges of flanges, spaced taking into account the *e/d* ratio, defined as the center-to-center spacing of the stiffeners divided by the depth of section. The considered *e/d* ratios were 3, 5, 7 and 9, which represents spacings between stiffeners of 102, 170, 238 and 306 mm, respectively. The longitudinal stiffeners consisted in aluminum plates of width, b_s = 25.4 mm, corresponding to 85% of the flange width b_f, and thickness equal to the section's web thickness t_w as shown in the Figure 4. For each test length and e/d ratio, six specimens were considered, three with longitudinal stiffeners and three without stiffeners, for a total of 192 tests.

Test setup and instrumentation

A beam specimen example and its test setup are shown in the Figure 5(a). Aluminum beams were supported on a 2.5" x 2.5" x ¼" steel L section (63 mm x 63 mm x 6 mm), which was bolted to an IPE 330 section.

Figure 5. Experimental program. **a)** Test setup; **b)** Detail of simply support. (Self-Elaboration).

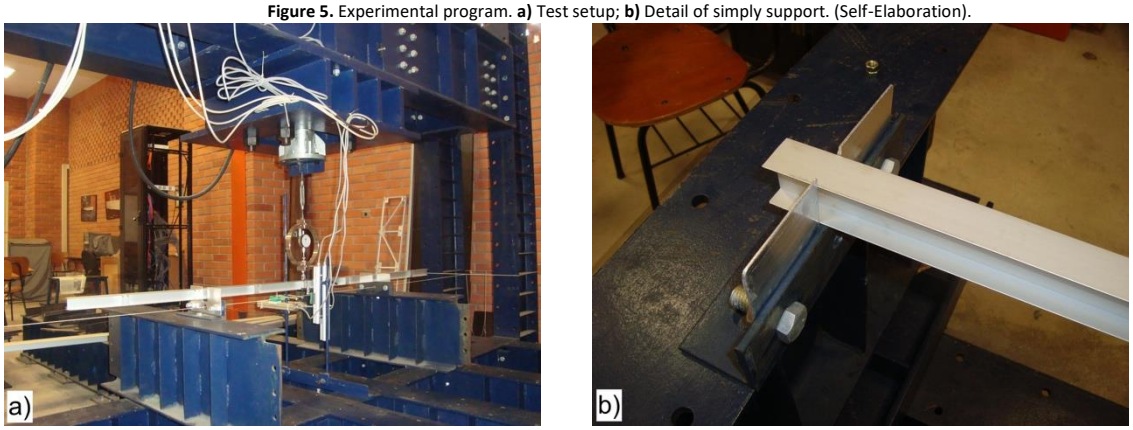

Additionally, an aluminum plate was bolted to the L section to provided full lateral restraint as shown in Figure 5(b). All specimens were tested as simply supported beams with point load at mid-span applied with a 200 kN capacity actuator. These test conditions produce that the moment value at the middle of the laterally unbraced length L_b to be greater than the moment values at the ends of the beam, which allow to take conservatively the value of moment gradient, C_b = 1.0, according with the specifications of ANSI/AISC 360 (American Institute of Steel Construction, 2016). The mid-span loading point allowed the lateral-torsional buckling of the section and the tests were carried out monotonically and load-controlled until failure of the specimens. Since the test considered an overall scaling of 1:9, it was necessary to include a 5 kN load ring between the hydraulic actuator and the specimen. This load ring allowed a better accuracy in measuring the applied load, which was recorded each 0.01 kN. The specimens were instrumented by using 5 displacement transducers. In this case, the displacement transducers were placed at mid-span to record vertical and horizontal displacement of top and bottom flanges, and vertical web displacement of the I-shaped section as shown in Figure 6. Finally, data acquisition from displacement transducers were recorded digitally by a computer. Table 4 shows the average values of measured maximum bending moments in all specimens.

Figure 6. Instrumentation of specimens. (Self-Elaboration).

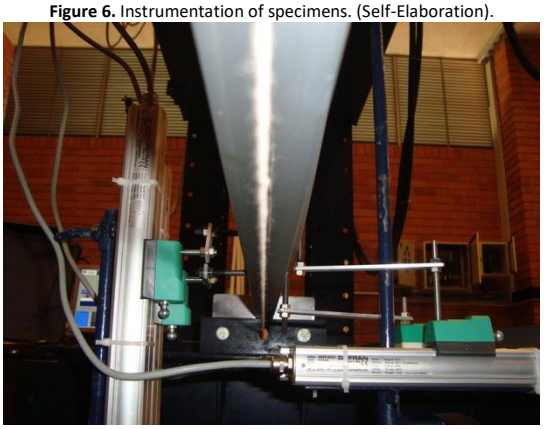

Table 4. Theoretical and measured moment. (Self-Elaboration).

Specimen	Moment (N·m)							
	L_b 0.55 m	L_b 0.80 m	L_b 1.00 m	L_b 1.20 m	L_b 1.40 m	L_b 1.60 m	L_b 1.80 m	L_b 1.95 m
Theoretical	120.0	97.8	82.2	63.3	51.1	43.3	36.7	33.3
Without stiffeners	141.6	106.6	78.3	73.2	58.2	47.8	39.8	34.1
e/d = 9	152.6	110.4	93.1	88.7	75.6	60.3	53.8	49.3
e/d = 7	152.6	123.2	102.2	91.6	76.6	63.4	53.8	48.3
e/d = 5	145.0	118.2	101.8	92.2	79.7	67.3	58.2	53.1
e/d = 3	164.1	134.4	101.9	94.4	85.4	74.7	62.1	57.8

Results and discussion

Figure 7 shows the relationship between bending moment and laterally unbraced length L_b of a theoretical beam and the tested specimens.

Figure 7. Theoretical and measured moment. (Self-Elaboration).

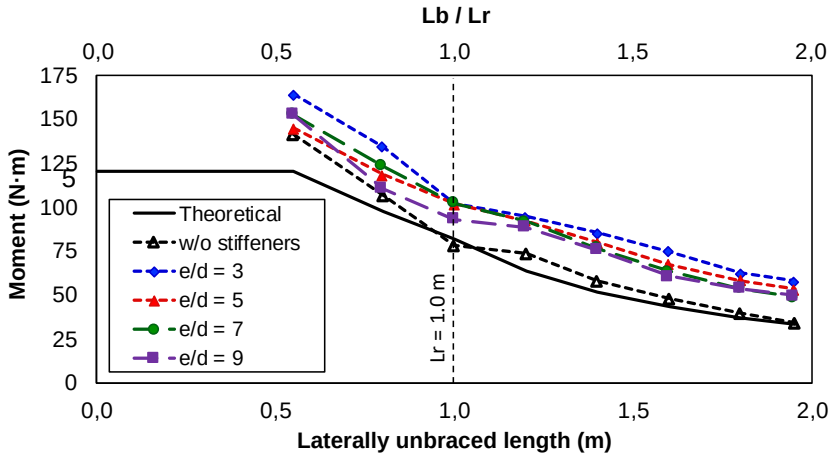

The theoretical moment (solid line) was calculated according to Eqs. 11 to 17 corresponding to the specifications of ANSI/AISC 360 (2016) for I-shaped beams with compact webs and noncompact flanges.

For inelastic buckling zone,

$$M_n = C_b \left[M_p - \left(M_p - 0.7 f_y S_x \right) \left(\frac{L_b - L_p}{L_r - L_p} \right) \right] \tag{11}$$

Where,

$$L_p = 1.76 r_y \sqrt{\frac{E}{f_y}} \tag{12}$$

$$L_r = 1.95 r_{ts} \frac{E}{0.7 f_y} \sqrt{\frac{Jc}{S_x h_o} + \sqrt{\left(\frac{Jc}{S_x h_o} \right)^2 + 6.76 \left(\frac{0.7 f_y}{E} \right)^2}} \tag{13}$$

c = Coefficient equal to 1.0 for doubly symmetric I-shaped beams.

This value should not be greater than the value obtained according to the limit state of compression flange local buckling,

$$M_n = C_b\left[M_p - \left(M_p - 0.7f_y S_x\right)\left(\frac{\lambda - \lambda_{pf}}{\lambda_{rf} - \lambda_{pf}}\right)\right] \quad (14)$$

Where,
λ, λ_{pf} and λ_{rf} are listed in Table 3.

For elastic buckling zone,

$$M_n = F_{cr} S_x \quad (15)$$

Where,

$$F_{cr} = \frac{C_b \pi^2 E}{(L_b/r_{ts})^2}\sqrt{1 + 0.0078\frac{Jc}{S_x h_o}\left(\frac{L_b}{r_{ts}}\right)^2} \quad (16)$$

$$r_{ts}^2 = \frac{\sqrt{I_y C_w}}{S_x} \quad (17)$$

The values of the specimens without stiffeners and different *e/d* ratio (dashed line), correspond to average measured moment of the tested specimens. The reached moment by the specimens with different *e/d* ratios was higher than those without longitudinal stiffeners. The highest values of bending moment capacity were reached by the specimen with a ratio of *e/d* = 3, meanwhile the lowest values were developed by the specimen with a ratio of *e/d* = 9. The specimens' bending moment without longitudinal stiffeners presented good agreement with respect to theoretical flexural capacity.

In order to validate the experimental results of this research carried out at 1:9 scale, the measured moment vs laterally unbraced length L_b of the specimens without longitudinal stiffeners and with a ratio e/d = 3 were normalized and compared with the experimental results performed on a real scale in the work carried out by (Prado et al., 2018) as shown in Figure 8.

Figure 8. Normalized measured moment. **a)** Specimens without stiffeners; **b)** Specimens with stiffeners. (Self-Elaboration).

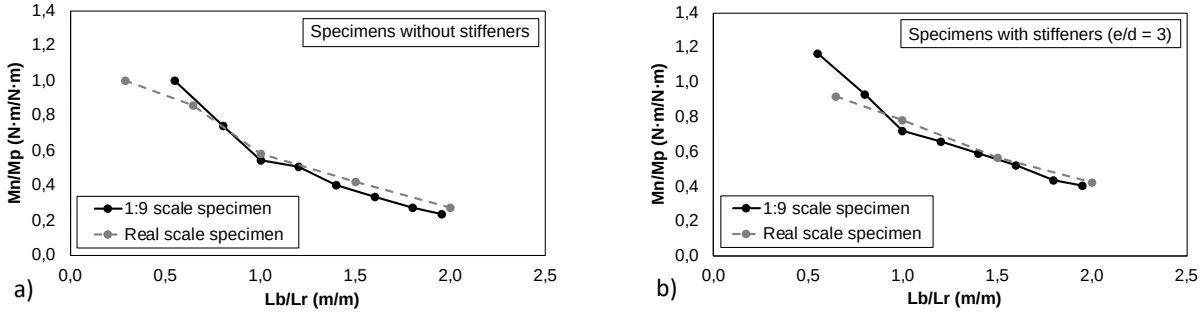

Figure 8 shows a good concordance of the values of measured moment of the specimens tested at real scale and 1:9 scale in the inelastic and elastic buckling zone, validating the experimental results of this research, whereas in the plastic buckling zone, the measured moment values are associated to the material strength.

The percentage of the measured moment increase of the specimens for the different *e/d* ratios with respect to the specimens without stiffeners are shown in Figure 9. The highest increment of the flexural moment was reached by the specimen with a ratio *e/d* = 3 and laterally unbraced length, L_b = 1.95 m. This specimen showed an increase of 72% with respect to the specimen without longitudinal stiffeners. On the other hand, the specimen with a ratio *e/d* = 9 and laterally unbraced length, L_b = 0.80 m showed an increase of 3%. The tests results indicate that for elastic buckling zone, the increase of bending moment capacity could be associated with the decrease of the *e/d* ratio and the increase of the laterally unbraced length L_b. Nevertheless, for plastic and inelastic buckling zones the above statement is not fully fulfilled.

Figure 9. Enhanced moment. (Self-Elaboration).

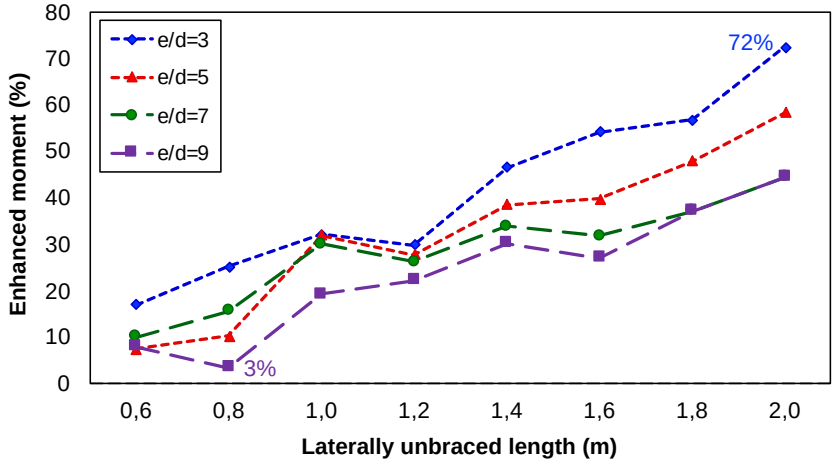

Figure 10 shows the measured moment vs. lateral displacement of the compression flange of all specimens. Despite of the lateral displacement of compression flange of all specimens stiffened was lower with respect to the specimens without longitudinal stiffeners, the lateral displacement did not display a tendency of behavior according to the different *e/d* spacing ratios of longitudinal stiffeners.

Figure 10. Lateral displacement of the compression flange. **a)** Specimens with Lb = 1.95 m; **b)** Specimens with Lb = 1.80 m; **c)** Specimens with Lb = 1.60 m; **d)** Specimens with Lb = 1.40 m; **e)** Specimens with Lb = 1.20 m; **f)** Specimens with Lb = 1.00 m; **g)** Specimens with Lb = 0.80 m; **h)** Specimens with Lb = 0.55 m. (Self-Elaboration)

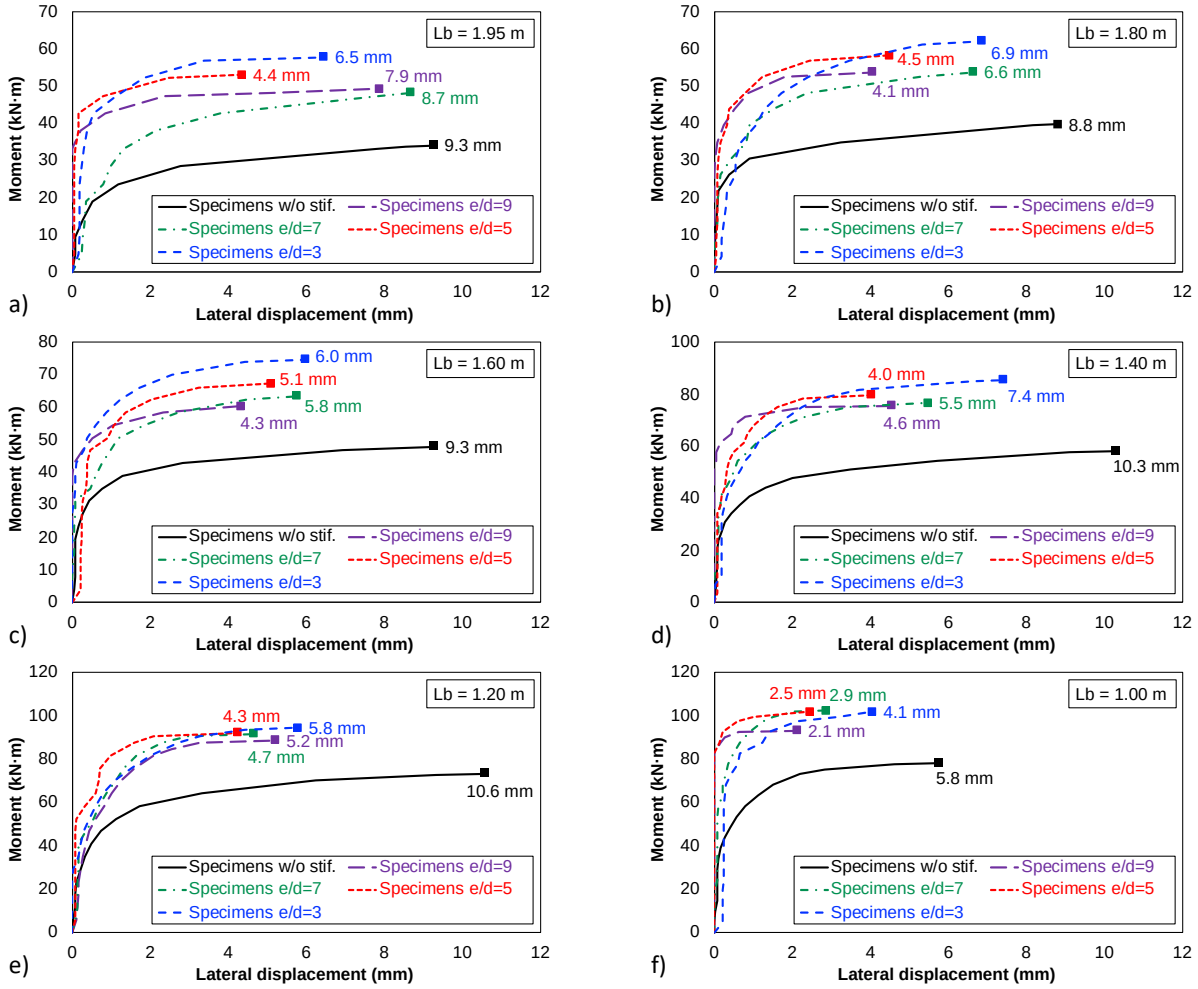

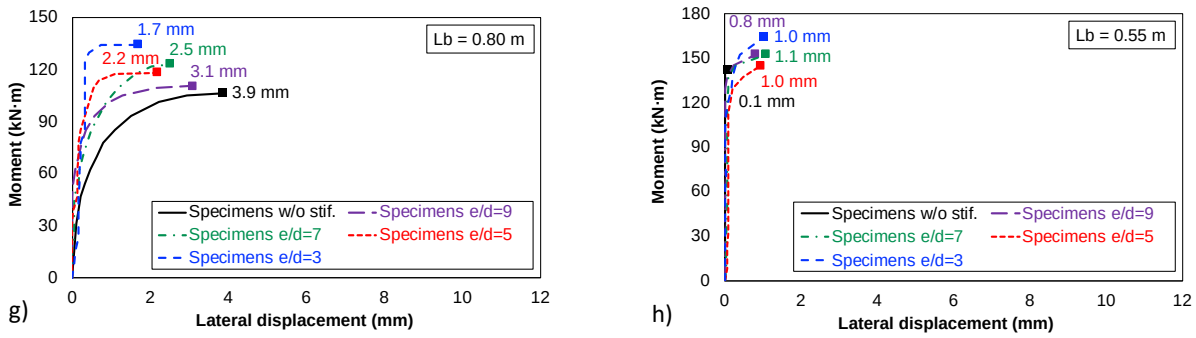

Since the measured twist angle of all specimens is calculated as the inverse sine function of the difference between the flanges' lateral displacement divided by the section's depth; it could be concluded that the different *e/d* spacing ratios of longitudinal stiffeners not evidence an behavior trend in the twist angle of the specimens.

During the tests, three types of failure modes in all specimens were identified. For laterally unbraced length, *Lb* = 0.80 m, which correspond to inelastic buckling zone, both specimens with stiffeners and without stiffeners developed buckling in the compression flange as shown in Figures 11(a). This failure mode matches what was discussed by (Yura et al., 1978), who indicated that the lateral-torsional buckling at the inelastic interval and local buckling in the compression flange occur, even if the beam has a suitable laterally unbraced length L_b to reach the plastic moment.

Figure 11. Modes failure examples. **a)** Local buckling of the flange; **b)** Inelastic lateral-torsional buckling; **c)** Elastic lateral-torsional buckling. (Self-Elaboration).

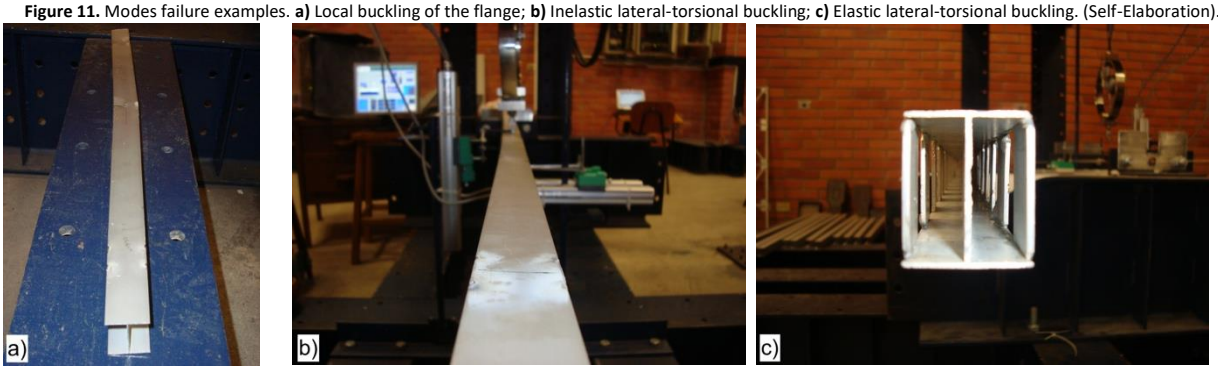

The failure mode of the specimens with laterally unbraced length, L_b = 1.00 m, was dominated by inelastic lateral-torsional buckling as shown in Figure 11(b). After load removal, these specimens kept a permanent deformation. This failure mode matches the characteristic described by the inelastic buckling zone (Salmon et al., 2009).

The failure mode of the specimens with laterally unbraced length L_b ranging from 1.20 up to 1.95 m was also dominated by lateral-torsional buckling. However, after load removal, these specimens did not display permanent deformation as show in Figure 11(c). The absence of residual deformations is an indication of elastic buckling (Salmon et al., 2009).

Conclusions

The performed tests in this research showed that the spacing of the longitudinal stiffeners on I-shaped beams influences the moment capacity of the section, especially in the elastic buckling zone. The lower spacing in the longitudinal stiffeners (the lower e/d ratio), the greater the moment capacity. The specimens stiffened reached an increase of the moment capacity to up 72, 58, 44 and 43% with respect to specimens without stiffened for e/d spacing ratio of 3, 5, 7 and 9, respectively. In addition, it was evidenced that for each e/d spacing ratio of longitudinal stiffeners, the percentage of improved moment exhibited a trend to increase when laterally unbraced length L_b increased.

Although the use of longitudinal stiffeners on I-shaped beams with different spacings decreased the lateral displacement of the compression flange, it was not evidenced a behavior trend of lateral displacement of the compression flange according to the e/d spacing ratio of longitudinal stiffeners arranged in the specimens.

Different e/d spacing ratios of longitudinal stiffeners did not evidence a behavior trend in the failure twist angle of the specimens, since the measured twist angle depends on the values obtained from the lateral displacement of compression flange.

Based on the experimental results of this study, an e/d spacing ratio of 3 of longitudinal stiffeners on I-shaped beams provided the best percentage of improved moment in the elastic buckling zone and even in the inelastic buckling zone.

References

American Institute of Steel Construction. (2016). *Specification for Structural Steel Buildings* (ANSI/AISC 360-16, p. 676) [American National Standard]. American Institute of Steel Construction. https://www.aisc.org/globalassets/aisc/publications/standards/a360-16-spec-and-commentary.pdf

American Society for Testing and Materials, A01 Committee. (2016). *Specification for General Requirements for Rolled Structural Steel Bars, Plates, Shapes, and Sheet Piling* (ASTM A6 / A6M - 16a, p. 63) [Standard]. ASTM International. https://doi.org/10.1520/A0006_A0006M-16A

American Society for Testing and Materials, B07 Committee. (2015). *Test Methods for Tension Testing Wrought and Cast Aluminum- and Magnesium-Alloy Products* (ASTM B557 - 15, p. 16) [Standard]. ASTM International. https://doi.org/10.1520/B0557-15

Cakiroglu, C., Bekdaş, G., Kim, S., & Geem, Z. W. (2020). Optimisation of Shear and Lateral–Torsional Buckling of Steel Plate Girders Using Meta-Heuristic Algorithms. *Applied Sciences*, *10*(10), 3639. https://doi.org/10.3390/app10103639

Gere, J. M., & Goodno, B. J. (2013). *Mechanics of Materials* (8th ed.). Cengage Learning.

Heins, C. P., & Potocko, R. A. (1979). Torsional Stiffening of I-Girder Webs. *Journal of the Structural Division*, *105*(8), 1689–1698.

Hotchkiss, J. G. (1966). Torsion of Rolled Steel Sections in Building Structures | American Institute of Steel Construction. *Engineering Journal*, *3*, 19–45.

Mamazizi, S., Crocetti, R., Mehri, H., & University, L. (2013). *Numerical and Experimental Investigation on the Post-Buckling Behavior of Steel Plate Girders Subjected to Shear*. 11.

Murtha-Smith Erling. (1995). Cross Stiffeners for Beams in Torsion. *Journal of Structural Engineering*, *121*(7), 1119–1124. https://doi.org/10.1061/(ASCE)0733-9445(1995)121:7(1119)

Ojalvo, M. (1975). Discussion of Warping and distortion at I-section joint, by Vacharajittiphan P., & Trahair N. S. *Journal of the Structural Division*, *101*(1), 343–345.

Ojalvo, M. (1980). Discussion of Torsional stiffening of I-girder webs, by Heins C. P., & Potocko R. A. *Journal of the Structural Division*, *106*(4), 939.

Ojalvo, M., & Chambers, R. S. (1977). Effect of warping restraints on I-beam buckling. *Journal of the Structural Division*, *103*(12), 2351–2360.

Plum Carsten M., & Svensson Sven Eilif. (1993). Simple Method to Stabilize I-Beams against Lateral Buckling. *Journal of Structural Engineering*, *119*(10), 2855–2870. https://doi.org/10.1061/(ASCE)0733-9445(1993)119:10(2855)

Prado, N. I., Carrillo, J., Ospina, G. A., & Ramirez-Amaya, D. (2018). Experimental assessment of I-shaped steel beams with longitudinal stiffeners under lateral-torsional buckling. *DYNA*, *85*(207), 278–287. https://doi.org/10.15446/dyna.v85n207.71892

Salmon, C. G., Johnson, J. E., & Malhas, F. A. (2009). *Steel Structures: Design and Behavior, 5th Edition*. /content/one-dot-com/one-dot-com/us/en/higher-education/program.html

Szewczak Richard M., Smith Erling A., & DeWolf John T. (1983). Beams with Torsional Stiffeners. *Journal of Structural Engineering*, *109*(7), 1635–1647. https://doi.org/10.1061/(ASCE)0733-9445(1983)109:7(1635)

Takabatake, H. (1988). Lateral buckling of I beams with web stiffeners and batten plates. *International Journal of Solids and Structures*, *24*(10), 1003–1019. https://doi.org/10.1016/0020-7683(88)90104-7

Takabatake Hideo, Kusumoto Shigeru, & Inoue Tomitaka. (1991). Lateral Buckling Behavior of I Beams Stiffened with Stiffeners. *Journal of Structural Engineering*, *117*(11), 3203–3215. https://doi.org/10.1061/(ASCE)0733-9445(1991)117:11(3203)

Vacharajittiphan, P., & Trahair, N. S. (1974). Warping and Distortion at I-Section Joints. *Journal of the Structural Division*, *100*(3), 547–564.

Vacharajittiphan, P., & Trahair, N. S. (1975). Closure to Warping and distortion at I-section joints. *Journal of the Structural Division*, *101*(8), 1703–1705.

Yura, J. A., Ravindra, M. K., & Galambos, T. V. (1978). The Bending Resistance of Steel Beams. *Journal of the Structural Division*, *104*(9), 1355–1370.